Interannual Variability of High-Wind Occurrence over the North Atlantic*

XUHUA CHENG

State Key Laboratory of Tropical Oceanography, South China Sea Institute of Oceanology, Chinese Academy of Sciences, Guangzhou, China, and International Pacific Research Center, University of Hawaii at Manoa, Honolulu, Hawaii

SHANG-PING XIE

International Pacific Research Center, University of Hawaii at Manoa, Honolulu, Hawaii, and Ocean University of China, Qingdao, China

HIROKI TOKINAGA

International Pacific Research Center, University of Hawaii at Manoa, Honolulu, Hawaii

YAN DU

State Key Laboratory of Tropical Oceanography, South China Sea Institute of Oceanology, Chinese Academy of Sciences, Guangzhou, China

(Manuscript received 18 October 2010, in final form 31 May 2011)

ABSTRACT

Interannual variability of high-wind occurrence over the North Atlantic is investigated based on observations from the satellite-borne Special Sensor Microwave Imager (SSM/I). Despite no wind direction being included, SSM/I data capture major features of high-wind frequency (HWF) quite well. Climatology maps show that HWF is highest in winter and is close to zero in summer. Remarkable interannual variability of HWF is found in the vicinity of the Gulf Stream, over open sea south of Iceland, and off Cape Farewell, Greenland. On interannual scales, HWF south of Iceland has a significant positive correlation with the North Atlantic Oscillation (NAO). An increase in the mean westerlies and storm-track intensity during a positive NAO event cause HWF to increase in this region. In the vicinity of the Gulf Stream, HWF is significantly correlated with the difference between sea surface temperature and surface air temperature (SST − SAT), indicative of the importance of atmospheric instability. Cross-frontal wind and an SST gradient are important for the instability of the marine atmospheric boundary layer on the warm flank of the SST front. Off Cape Farewell, high wind occurs in both westerly and easterly tip jets. Quick Scatterometer (QuikSCAT) data show that variability in westerly (easterly) HWF off Cape Farewell is positively (negatively) correlated with the NAO.

1. Introduction

High marine winds are a great threat to maritime activity and to coastal communities. High winds also have beneficial effects: they stir up nutrients from below the mixed layer into the euphotic layer and spawn plankton blooms (Lin et al. 2003). In coastal regions, steady winds are an increasingly important energy resource (Barthelmie and Pryor 2003). High winds are also associated with intense air–sea fluxes of heat, moisture, and momentum—processes important in forcing ocean currents and shaping climate (Moore and Renfrew 2005; Soloviev and Lukas 2006). Monitoring frequency of high winds (speed >20 m s^{-1}) is not only useful for scientific research in oceanography, meteorology, and climate science but also is of applied value for navigation safety and coastal disaster prevention (Sampe and Xie 2007).

With the availability of high-resolution satellite wind data, several works have been focused on high-wind

* International Pacific Research Center/School of Ocean and Earth Science and Technology Publication Number 791/8198.

Corresponding author address: Xuhua Cheng, State Key Laboratory of Tropical Oceanography, South China Sea Institute of Oceanology, Chinese Academy of Sciences, 164 West Xingang Road, Guangzhou 510301, China.
E-mail: xuhuacheng@scsio.ac.cn

DOI: 10.1175/2011JCLI4147.1

frequency (HWF) on both planetary and regional scales. Yuan (2004) examined the spatial and seasonal variability of high wind characteristics in the Southern Ocean. She found that high wind only accounts for 1% of the total wind observations during the study period. Using the 10-m wind field dataset from the Quick Scatterometer (QuikSCAT), Moore and Renfrew (2005) developed the wintertime climatology of high wind events in the vicinity of Greenland based on twice-daily 10-m wind speed and direction data from the SeaWinds scatterometer. They showed that high wind events (>25 m s^{-1}) occur up to 15% of the time off Cape Farewell and up to 10% of the time in Denmark Strait. Based on 5-yr QuikSCAT satellite measurements, Risien and Chelton (2006) presented climatological maps of global ocean winds and wind rose plots. Through the maps, the influence of sea surface temperature (SST) fronts on surface winds is clearly observed in regions such as the southwest Indian and northwest Atlantic Ocean. Sampe and Xie (2007) constructed a global climatology of HWF (>20 m s^{-1}) based on 7-yr QuikSCAT observations. The climatology maps show that high winds occur in the midlatitudes over the North Atlantic, North Pacific during boreal winter, and in the Southern Ocean during boreal summer. Among all oceans, high wind occurs most frequently over the North Atlantic during winter, especially off Cape Farewell.

Over the North Atlantic, the storm track is most intense in midwinter and extends from the east coast of America to Ireland, Great Britain, and Norway (Hoskins and Hodges 2002), along which synoptic-scale transient eddies contribute to an increase in HWF over the ocean (Sampe and Xie 2007). During winter the Gulf Stream anchors sharp SST fronts, on the warm flank of which high winds occur more frequently than over cold waters on the continental shelf/slope (Sampe and Xie 2007). This can be explained by the fact that SST fronts significantly alter the entire marine atmospheric boundary layer (MABL) and accelerate the wind on the warmer flank of SST fronts (Chelton et al. 2004; Xie 2004; Spall 2007; Minobe et al. 2008; Small et al. 2008). Orography can also cause high winds near the coast, for example, at the south tip of Greenland, south of France, and west of Norway (Moore 2003; Pezzoli et al. 2004; Moore and Renfrew 2005; Sampe and Xie 2007).

These studies have focused on the climatology of HWF over the North Atlantic. To our knowledge, interannual variability of HWF has not been discussed in the literature. The North Atlantic Oscillation (NAO) is the dominant mode of atmospheric variability over the North Atlantic, whose effects on ocean circulation, surface wind, air–sea heat fluxes, and storm tracks have been studied extensively (Hurrell 1995; Rogers 1997; Hurrell et al. 2003; Visbeck et al. 2003). How the NAO influences the HWF on interannual time scales is still unclear. Recent observations of air–sea interaction over ocean fronts have revealed a positive correlation between SST and near-surface wind speed (e.g., Xie et al. 1998; Liu et al. 2000; Chelton et al. 2001; Hashizume et al. 2001; Thum et al. 2002; Nonaka and Xie 2003; O'Neill et al. 2003; Tokinaga et al. 2005). The hypothesized mechanisms for changes in the surface wind field in the vicinity of SST fronts include strong vertical turbulent mixing that brings down stronger wind from aloft (Wallace et al. 1989) and pressure-induced secondary circulation (Small et al. 2003; Spall 2007). See recent reviews by Small et al. (2008) and Chelton and Xie (2010). Are these mechanisms important for interannual variability in HWF?

The present study investigates interannual variability of HWF over the North Atlantic by taking advantage of satellite observations. First, we repeat the analysis by Sampe and Xie (2007) with the Special Sensor Microwave Imager (SSM/I) and confirm that the SSM/I data capture features of HWF fairly well. Covering more than 22 years, the SSM/I data are more suitable than the 10-yr-long QuikSCAT data to study interannual variability in HWF. We find that HWF displays strong interannual variations along the Gulf Stream, south of Iceland, and off Cape Farewell. These interannual variations of HWF are related to the NAO, MABL stability modulation induced by SST fronts, and orography.

The rest of the paper is organized as follows. Section 2 describes the satellite datasets and methods used for the analysis. Section 3 compares climatological maps of HWF between SSM/I and QuikSCAT data. Section 4 studies interannual variations of HWF and discusses their mechanisms. Section 5 is a summary and discussion.

2. Data and method

We use wind estimates from the SSM/I to study interannual variations of HWF. The SSM/I is a seven-channel, four-frequency, linearly polarized passive microwave radiometric system, flown on board the U.S. Air Force Defense Meteorological Satellite Program (DMSP) Block 5D-2 spacecraft. The instrument measures surface/atmospheric microwave brightness temperatures (T_B) at 19.35, 22.235, 37.0, and 85.5 GHz. The four frequencies are sampled in both horizontal and vertical polarizations, except for 22 GHz, which is sampled in the vertical only. With these channels, near-surface wind speed W (m s^{-1}), columnar water vapor V (mm), and columnar cloud liquid water L (mm) are retrieved from T_B (Hollinger 1989).

We use the wind speed product of Remote Sensing Systems (RSS) on a $0.25° \times 0.25°$ grid, which contains twice-daily maps derived from the T_B model function of

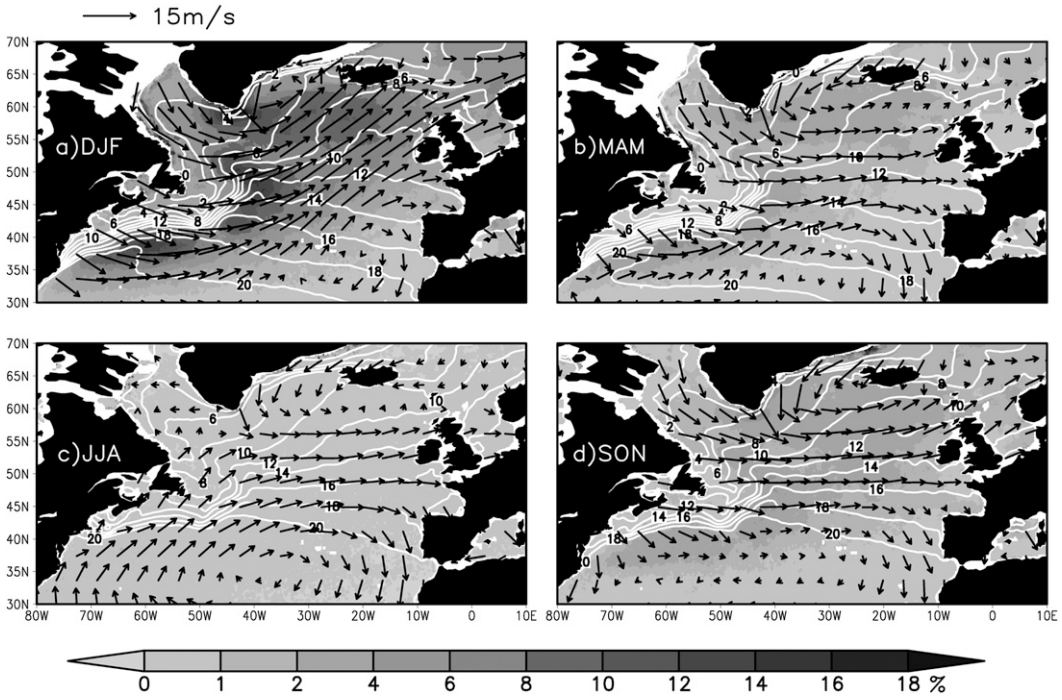

FIG. 1. Climatological seasonal means of high wind frequency (%) from SSM/I data for (a) winter (DJF), (b) spring (MAM), (c) summer (JJA), and (d) autumn (SON) superimposed on climatological seasonal means of AVHRR SST (white contours) and QuikSCAT wind velocity (arrows).

Wentz (1997). In the absence of rain, the inverse model provides wind retrievals with a rms accuracy of 0.9 m s^{-1}. The wind data analyzed here cover 22 years from January 1988 to December 2009. To keep uniform samples in every month, daily data from satellites *F08* (January 1988–December 1991), *F11* (January 1992–December 1999), and *F13* (January 2000–November 2009) are used. Wind observations with rain flags are abandoned to avoid possible contamination by rain. Removal of rain-flagged data may slightly underestimate the frequency of high winds because high winds often accompany intense rain. At each grid point and for each calendar month, we count the ratio (in percentage) between the number of observations with wind speeds greater than 20 m s^{-1} and the total number of valid wind observations in the twice-daily data. For comparison, HWF is also estimated for each month using the QuikSCAT vector wind product of RSS from July 1999 to November 2009. Detailed descriptions of QuikSCAT data may be found in Wentz et al. (2001) and Sampe and Xie (2007). QuikSCAT measures both wind speed and direction and yields observations twice daily at middle and high latitudes. Although the SSM/I data do not include directional information and are less frequent in coverage than QuikSCAT, their long record of 22 years (versus 10 years for QuikSCAT) makes SSM/I more suitable to study interannual variations of HWF.

To compute the cross-frontal wind and storm-track intensity, we use the 10-m winds from the National Centers for Environmental Prediction (NCEP)–National Center for Atmospheric Research (NCAR) atmospheric reanalysis (Kalnay et al. 1996). The optimal interpolation sea surface temperature (OISSTv2) analysis product is used to calculate the SST gradient. The OISSTv2 analyses are based on Advanced Very High Resolution Radiometer (AVHRR) infrared satellite SST data and have a spatial resolution of 0.25° and temporal resolution of 1 day (Reynolds et al. 2002, 2007). For near-surface atmospheric instability, climatological turbulent heat fluxes and the difference between SST and air temperature are calculated using ship observations in the International Comprehensive Ocean–Atmosphere Dataset (iCOADS) release 2.1 (Worley et al. 2005).

3. HWF climatology

Figure 1 displays the climatological mean distribution of HWF for each season, winter [December–February (DJF)], spring [March–May (MAM)], summer [June–August (JJA)], and autumn [September–November (SON)]. The climatology is defined as a 22-yr average over the period from 1988 to 2009. In winter high winds occur frequently in the vicinity of the Gulf Stream, off Cape Farewell, and south of Iceland. The high wind frequency in all of these

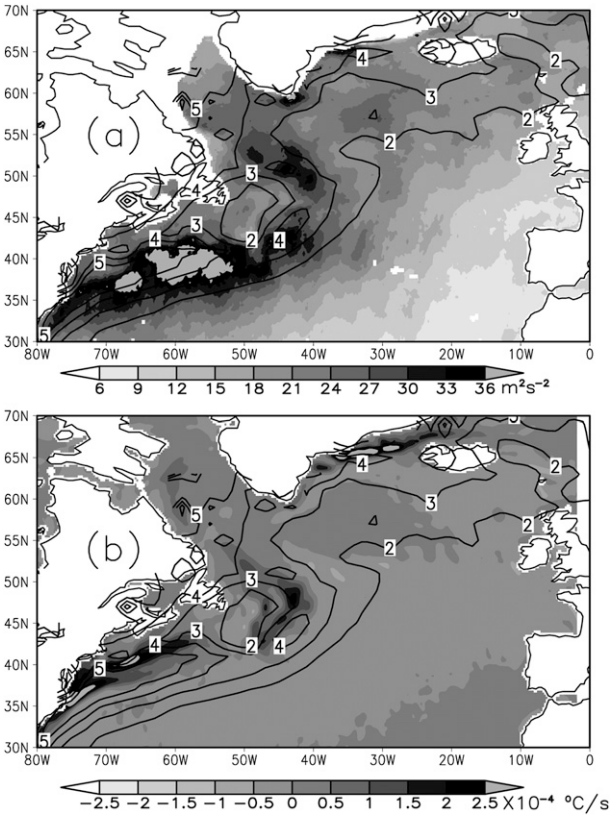

FIG. 2. Winter climatology of (a) storm track intensity ($m^2\ s^{-2}$) and (b) cross-frontal advection ($\mathbf{U} \cdot \nabla T$, 10^{-4}°C s^{-1}) superimposed on SST − SAT difference (black contour: 1°C interval). Storm-track intensity is measured by eddy kinetic energy $(u'^2 + v'^2)/2$ from QuikSCAT data.

regions exceeds 10%, especially off Cape Farewell where it is more than 18%. The HWF pattern shown in Fig. 1a matches the result of Sampe and Xie (2007, their Fig. 2a), which indicates that the SSM/I data capture the high wind occurrence very well. The HWF patterns in spring and autumn are similar to those in winter with the magnitude reduced to only ~2%. In summer, HWF is close to zero over the whole basin.

In winter, the mean winds are mostly northwesterly off North America and southwesterly in the midbasin with a speed of 10–15 m s^{-1} in the central basin (Fig. 1a). In addition, storm tracks are intense along the Gulf Stream (Fig. 2a) where the boundary layer is usually unstable (Booth et al. 2010). Synoptic-scale transient eddies along storm tracks can cause high wind. Therefore, both the increase in westerly wind and enhancement of storm-track intensity in winter contribute to an increase in HWF (Sampe and Xie 2007). The sharp SST front associated with the Gulf Stream also contributes to the HWF on the warm flank of the SST front by reducing MABL stability (Figs. 1a,b,d). In the vicinity of an SST front, the gradient of the sea air temperature (SAT) is much smoother than the SST gradient due to the disparity in horizontal scale between atmospheric adjustment and oceanic fronts (Rogers 1989; Warner et al. 1990; Sampe and Xie 2007). Therefore, SST is higher than SAT on the warmer flank of front. When SST − SAT is positive, the MABL grows unstable, which favors the increase of surface wind as winds blow from the cold flank of an SST front to the warm flank (O'Neill et al. 2003; Chelton et al. 2004; Xie 2004; Tokinaga et al. 2005; Small et al. 2008; Spall 2007). As shown in Fig. 2a, SST − SAT is 3°–5°C on the warmer flank in winter, indicating high instability within the MABL. As a result, HWF on the warmer flank is about 10% higher than that over the cold coastal waters, and the mean wind is 4 m s^{-1} higher over the warmer side.

Previous studies indicate that stability of the MABL near the front also depends on the mean cross-frontal wind (Wallace et al. 1989; Xie 2004). In this study, we use the wind velocity multiplied by downwind SST gradient ($\mathbf{U} \cdot \nabla T$) to measure cross-frontal thermal advection and its effect on MABL stability, following Chelton et al. (2001). As shown in Fig. 2b, $\mathbf{U} \cdot \nabla T$ is positive along the SST front during winter, accompanied by high SST − SAT and HWF on the warmer side.

To illustrate the annual cycle of the cross-frontal variations in HWF, SST − SAT, turbulent heat fluxes ($Q_S + Q_L$), cross-frontal advection ($\mathbf{U} \cdot \nabla T$), and storm-track intensity (eddy kinetic energy of wind fluctuations with period < 8 days), Fig. 3 shows cross-frontal variations of them along 48°N. Except in summer, $\mathbf{U} \cdot \nabla T$ is high within the frontal zone. Consistent with the hypothesis for atmospheric adjustment to a narrow SST front (Xie 2004), the MABL changes from stable to unstable as the wind blows from the cold to warm flank of an SST front (Fig. 3). In winter, SST − SAT is 1°C and turbulent heat flux is ~80 W m^{-2} on the cold side of the front. Within the frontal zone, HWF, SST − SAT, $Q_S + Q_L$, and storm-track intensity increase remarkably. Their maxima are found on the warm side of the frontal region. The maximum of SST − SAT is about 4°C and $Q_S + Q_L$ reaches a maximum of about 280 W m^{-2} (Figs. 3b,c). HWF increases to about 12% on the warm side of the SST front (Fig. 3a). In spring and autumn the cross-frontal increases in SST − SAT and $Q_S + Q_L$ are about 2°C and ~80 W m^{-2}. The HWF increase is about 2%–4%. During summer all variables are small with little cross-frontal variations.

4. Interannual variations

The seasonal climatology in the vicinity of the Gulf Stream indicates a great impact of SST fronts on MABL stability and HWF. This section extends the HWF analysis to interannual time scales. As the high wind

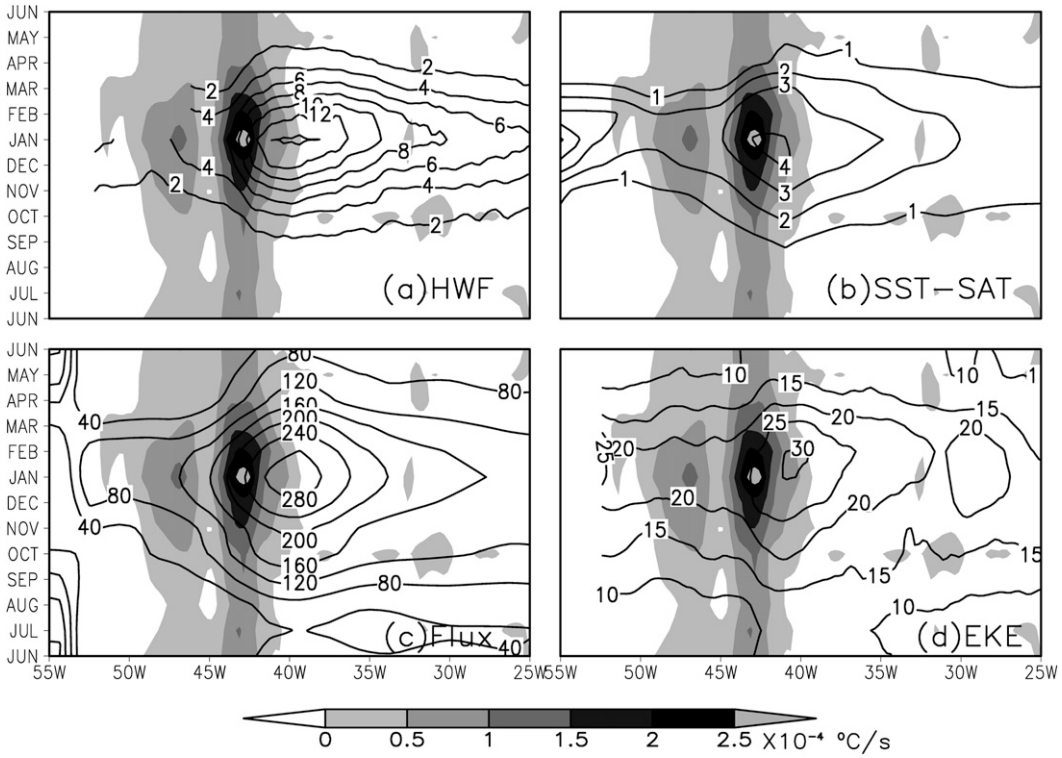

FIG. 3. Climatological annual cycle along 48°N: (a) high-wind frequency (%), (b) SST − SAT (°C) from ICOADS data, (c) turbulent heat fluxes (W m^{-2}), and (d) EKE $[(u'^2 + v'^2)/2]$ from QuikSCAT data The grayscale shading is for cross-front advection ($\mathbf{U} \cdot \nabla T$, 10^{-4}°C s^{-1}).

events happen most frequently in winter, we focus on the interannual variations of winter HWF. Figure 4 depicts the standard deviation (STD) of interannual HWF anomalies for the period from 1988 to 2009 based on SSM/I data (Fig. 4a) and for the period from 1999 to 2009 based on QuikSCAT data (Fig. 4b). All time series at each labeled grid box in Fig. 4 have been detrended using linear least squares regression. Over large portions of the basin, a rather good quantitative agreement is found between the two. High variability of HWF is found south of Iceland, off Cape Farewell, and in the vicinity of the Gulf Stream. Two bands of high variance are found off Cape Farewell, extending southwestward and eastward, respectively (Fig. 4b). Regions A, B, and C in Fig. 4 denote high variance areas influenced by SST fronts. Here, D is a region south of Greenland with strong orographic effects, and E is an open sea area of high variability. As we will demonstrate later, HWF in these regions display different interannual variations owing to a different mechanism.

a. NAO effect

Over the middle- and high-latitude Northern Atlantic, the NAO is the most prominent recurrent pattern of atmospheric variability (Hurrell 1995; Hurrell et al. 2003; Visbeck et al. 2003). When the NAO is in its positive phase, SST displays a tripole pattern with a cold anomaly in the subpolar region, a warm anomaly in the middle latitudes, and a cold subtropical anomaly between the equator and 30°N (e.g., Deser and Blackmon 1993; Visbeck et al. 2001, 2003; Tanimoto and Xie 2002). There are also stronger-than-average surface westerlies across the middle latitude Atlantic to Europe during positive NAO, as well as more frequent and stronger winter storms crossing the Atlantic Ocean on a more northerly track (Hurrell and van loon 1997; Rogers 1997; Hurrell et al. 2003; Visbeck et al. 2003). This subsection discusses how the NAO influence HWF in the North Atlantic Ocean.

Figure 5 shows the regression of HWF and NCEP–NCAR reanalysis 10-m wind upon the normalized NAO index (Hurrell 1995) over the North Atlantic Ocean (NAO index is downloaded from http://www.cpc.ncep.noaa.gov/data/teledoc/nao.shtml). Significant HWF anomalies are found in two bands: one centered at ~57°N and the other at ~37°N. In the north band the HWF regression coefficients are 2%–6%, with a maximum south of Iceland (region E). In the south band there is a negative relationship between the NAO and HWF, and the regression

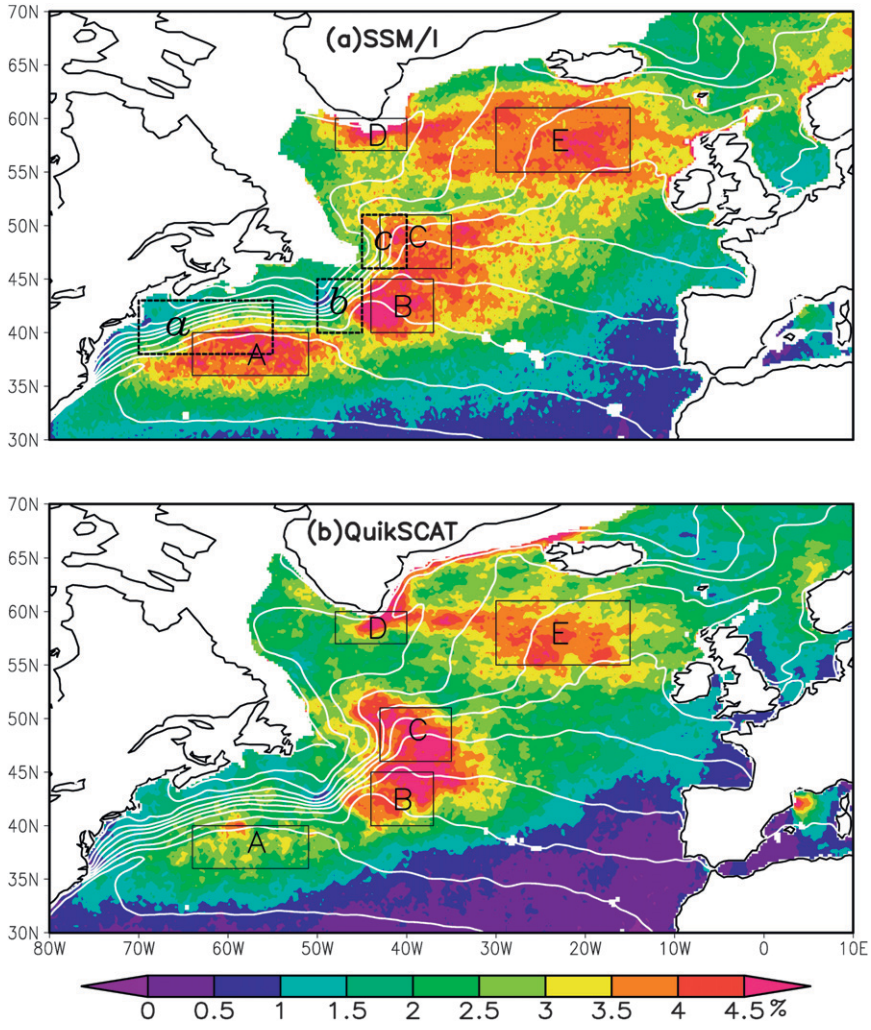

FIG. 4. Interannual standard deviation of winter (DJF) high wind frequency (color, %) based on (a) SSM/I data and (b) QuikSCAT data, respectively, superimposed on climatological seasonal means of AVHRR SST (white contours).

coefficients are between −2% and −5%. The maximum wind response to the NAO is in the north band with a regression coefficient of about 2 m s^{-1}. When the NAO index is positive, an increase in the mean westerly wind contributes to the increase in HWF in this region. As for the storm track, its intensity has a positive correlation with the NAO in the north band and a negative correlation in the south (Fig. 5). The wind speeds in extratropical cyclones along the storm track occasionally exceed 20 m s^{-1}, so enhanced storm-track intensity during the positive NAO phase contributes to the increase in HWF.

Figure 6 shows the time series of HWF, mean wind, and storm-track intensity averaged for area south of Iceland (region E in Fig. 4). On the interannual time scale, HWF averaged in the region has a remarkable positive correlation with the NAO (r = 0.71, the 95% significance level r_{95} = 0.32). The correlation between HWF and mean wind speed (storm-track intensity) is 0.66 (0.44). Mean wind (storm-track intensity) is correlated with the NAO at 0.68 (0.58), which exceeds the 95% significance level (Table 1). The significant correlations among these variables suggest that the NAO influences HWF in this region by altering mean westerlies and storm-track intensity.

b. *Influence of SST fronts*

Interannual variability of HWF is large on the warm flank of the Gulf Stream front. This subsection investigates its cause. Regions A and B near the Gulf Stream are affected by NAO (Fig. 5). The correlation between the NAO and HWF in region A (region B) is −0.43 (−0.36),

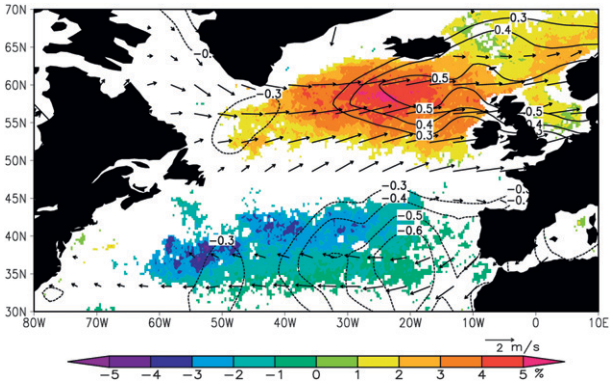

FIG. 5. Regression coefficients of high-wind frequency (color) and 10-m wind (vector) on the normalized NAO index in DJF. The high wind frequency and 10-m wind are based on SSM/I and NCEP reanalysis, respectively. Correlation coefficients of storm track intensity with the NAO index are indicated by black contours. The storm track intensity is measured by eddy kinetic energy from the NCEP 10-m wind.

above the 95% significance level (Table 2). HWF in region A (region B) is correlated with mean wind speed at 0.55 (0.74). However, the NAO has little impact on the mean wind speed in these two regions ($r = -0.27$ and -0.02). In region C, HWF has no significant correlation with the NAO ($r = -0.08$), while it has remarkable correlation with mean wind speed ($r = 0.72$). From above analysis, significant correlation is found between HWF and mean wind speed in the vicinity of the SST front. Mean westerly winds can impact the HWF in two ways. On the one hand, an increase in wind speed itself contributes to an increase in HWF (Sampe and Xie 2007). On the other, as an increased wind blows from the cold side of SST front to the warm side, it intensifies turbulent mixing in the MABL, and increases HWF (Wallace et al. 1989; Xie 2004).

Figure 7 shows the time series of HWF, SST − SAT averaged over region C, and $\mathbf{U} \cdot \nabla T$ averaged over the region c (in Fig. 4a). HWF in region C has a significant correlation with SST − SAT ($r = 0.66$, above 95% confidence level), indicating that atmospheric instability (SST − SAT) has a great impact on HWF on interannual time scales. HWF is even more highly correlated with $\mathbf{U} \cdot \nabla T$ in region c ($r = 0.79$). Previous studies suggest that cross-frontal winds and SST gradients are important to the instability of MABL on the warm flank of an SST front (e.g., Chelton et al. 2001). Unstable MABL on the warmer flank of the front with strong turbulent mixing brings down stronger winds from aloft, accelerating the surface wind (Wallace et al. 1989; Chelton et al. 2004; Xie 2004; Spall 2007; Small et al. 2008). As shown in Fig. 7, $\mathbf{U} \cdot \nabla T$ in region c is highly correlated with SST − SAT in the region ($r = 0.81$), in support of the above mechanism. In regions A and B, significant correlations among HWF, SST − SAT and $\mathbf{U} \cdot \nabla T$ also exist (Table 2). Moreover, SST − SAT ($\mathbf{U} \cdot \nabla T$) in region B is correlated with the NAO at −0.35 (−0.31), indicating that the NAO influences MABL instability and cross-frontal advection to some extent by changing the large-scale circulation. All of this then affects HWF.

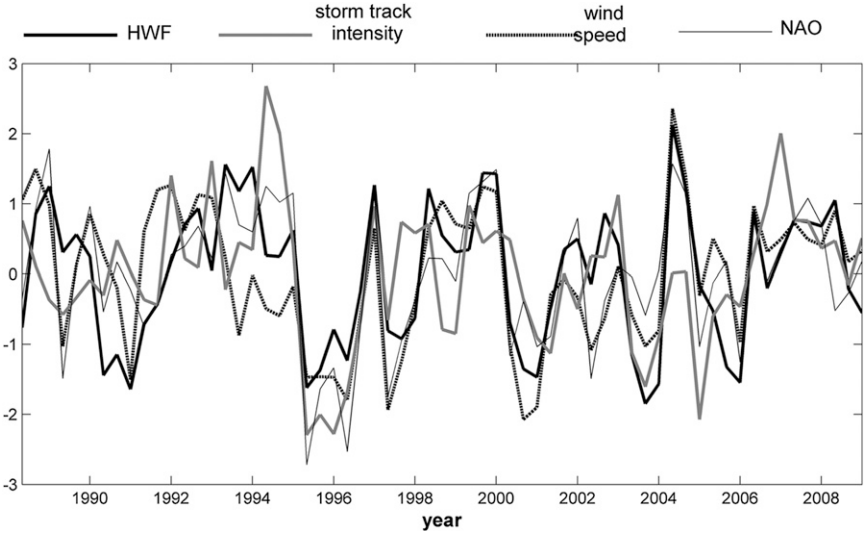

FIG. 6. Time series of DJF high wind frequency based on SSM/I data, mean wind speed, storm-track intensity anomalies averaged in region E (in Fig. 4a), and DJF NAO index. All time series are normalized by their respective standard deviations and have been detrended using linear least squares regression.

TABLE 1. Correlation coefficients between high wind frequency, wind speed, storm-track intensity averaged in region E, and winter NAO index (all coefficients satisfy the 95% confidence level criterion).

	HWF	Wind speed	Storm track	NAO index
HWF	1	0.66	0.44	0.71
Wind speed		1	0.40	0.68
Storm track			1	0.58
NAO index				1

TABLE 2. Correlation coefficients among winter NAO index, high wind frequency, wind speed, SST − SAT, $\mathbf{U} \cdot \nabla T$ in region A and B (coefficients in bold satisfy the 95% confidence level criterion).

	HWF	NAO	Wind speed	SST − SAT	$\mathbf{U} \cdot \nabla T$
			Region A		
HWF	1	**−0.43**	**0.55**	**0.58**	**0.42**
NAO		1	−0.27	−0.23	−0.20
Wind speed			1	**0.35**	0.23
SST − SAT				1	**0.79**
$\mathbf{U} \cdot \nabla T$					1
			Region B		
HWF	1	**−0.36**	**0.74**	**0.71**	**0.70**
NAO		1	−0.02	**−0.35**	−0.31
Wind speed			1	**0.53**	**0.54**
SST − SAT				1	**0.74**
$\mathbf{U} \cdot \nabla T$					1

To illustrate HWF variations associated with $\mathbf{U} \cdot \nabla T$, Fig. 8 presents a composite map based on $\mathbf{U} \cdot \nabla T$ time series in region c. The composite HWF difference between positive and negative phases of $\mathbf{U} \cdot \nabla T$ exhibits a positive maximum in region C with a value of 12%–15%, indicating that local $\mathbf{U} \cdot \nabla T$ can strongly affect HWF on the warm flank of the SST front on interannual time scales. The HWF difference is positive nearly everywhere in the vicinity of region C, whereas it is negative in the far southwest (region A). Composite 10-m wind fields display a cyclonic (anticyclonic) circulation in the north (south) in favor of the increase (decrease) in HWF over region C (region A). This pattern of large-scale circulation resembles surface wind anomalies associated with the east Atlantic (EA) pattern, known as the second prominent mode of low-frequency variability over the North Atlantic (Barnston and Livezey 1987; Josey and Marsh 2005). The EA pattern is characterized by a north–south dipole of anomaly centers displaced southeastward to the approximate nodal lines of the NAO pattern. We find that the EA mode has significant positive correlations with the HWF in region C (r = 0.64) and region B (r = 0.60) (not shown), whereas the NAO shows relatively weak correlations in both regions. These results suggest that the EA mode plays an important role in the interannual variations of HWF near the SST fronts.

c. *Interannual variations off Cape Farewell*

Off Cape Farewell (region D), the correlation between HWF and the NAO is not significant (r = 0.24), and the HWF correlations with storm-track intensity and mean wind speed are close to zero. As will be discussed in

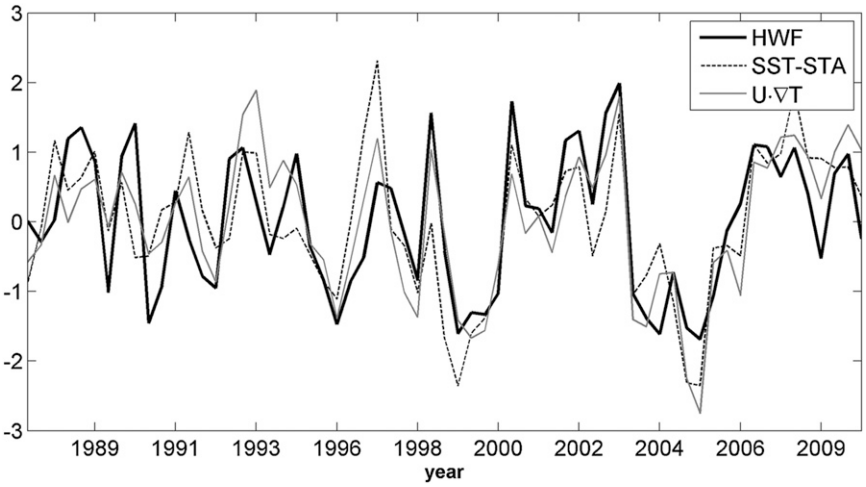

FIG. 7. Time series of DJF high wind frequency anomaly based on SSM/I data, SST − SAT anomaly averaged in region C, and $\mathbf{U} \cdot \nabla T$ anomaly averaged in region c (Fig. 4a). All time series are normalized by their respective standard deviations and have been detrended using linear least squares regression.

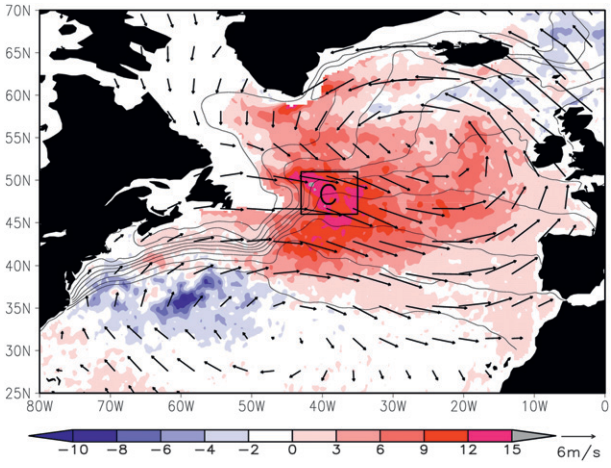

FIG. 8. Composite difference in HWF (color) and 10-m wind (vector) between positive and negative phases of $\mathbf{U} \cdot \nabla T$ anomaly in region c (Fig 4a) ($\mathbf{U} \cdot \nabla T > 1.0$ for positive, and $\mathbf{U} \cdot \nabla T < -1.0$ for negative), superimposed on climatological means of winter AVHRR SST (black contours). Nine positive and nine negative phases are included in the composite. The HWF and 10-m wind are based on SSM/I data and NCEP dataset, respectively.

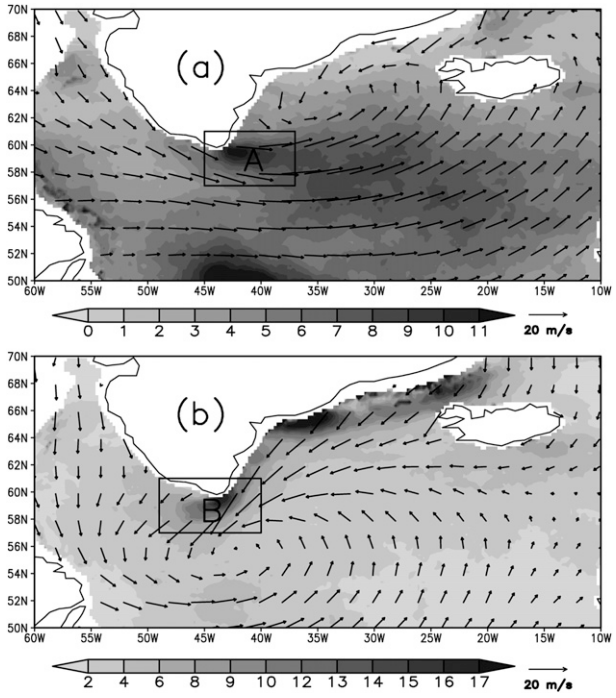

FIG. 9. Climatological means of high wind frequency (grayscale, %) and composite 10-m wind field (vectors) for winter (DJF) from QuikSCAT wind associated with (a) westerly and (b) easterly high wind events. The composite 10-m winds are constructed from daily QuikSCAT data when westerly and easterly wind speeds averaged over regions A and B are more than 20 m s^{-1}.

this subsection, the poor correlations are due to the alternate occurrence of westerly and easterly tip jets (also called tip jet and reverse tip jet) that develop downstream of the southern tip of Greenland. Both jets contribute to HWF variability (Moore 2003; Moore and Renfrew 2005).

The high topography of southern Greenland forces significant atmospheric flow distortion in coastal seas off Cape Farewell. The region near Cape Farewell is the windiest location in the World Ocean (Moore 2003; Sampe and Xie 2007; Moore et al. 2008; Renfrew et al. 2008). This is to a large extent due to the effect of Greenland topography on low pressure systems in winter (Doyle and Shapiro 1999; Hoskins and Hodges 2002; Moore 2003; Moore and Renfrew 2005). Doyle and Shapiro (1999) studied the dynamics of westerly tip jet that develop east of Cape Farewell using a numerical model. Moore (2003) examined both easterly and westerly tip jets off Cape Farewell using the NCEP reanalysis data. Using high resolution 10-m winds from the QuikSCAT scatterometer, Moore and Renfrew (2005) identified three wind regions: the westerly tip jet, easterly tip jet, and barrier flow. They suggested that each type of flow is the result of an interaction between a synoptic-scale parent cyclone and the high topography of Greenland. Renfrew et al. (2009) and Outten et al. (2009) described and modeled an easterly tip jet off Cape Farewell that occurred during the Greenland Flow Distortion Experiment.

Their studies suggest that westerly and easterly high-wind events occur alternately off Cape Farewell. Therefore it is helpful to separate high wind events into two types: one induced by westerly and the other by easterly winds. In this subsection, we use the QuikSCAT data because they include both wind speed and direction. At each grid point and for each calendar month, we obtain the westerly (easterly) HWF by computing the ratio between the number of westerly (easterly) observations with its speed exceeding 20 m s^{-1} and the total number of valid wind observations. As shown in Fig. 9a, westerly HWF is more than 11% off Cape Farewell in winter, with a tail extending eastward. The composite 10-m wind field during westerly high-wind events displays a cyclonic circulation north of 50°N with a center situated to the north and east of Cape Farewell. Easterly HWF reaches 17% off Cape Farewell and decreases toward the southwest, a cyclonic circulation centered to the south (Fig. 9b).

Pickart et al. (2003) found a greater number of westerly tip jet events during positive rather than negative NAO winters. Using NCEP analysis 1948–2000, Moore (2003) showed that the probability of westerly tip jet (easterly tip jet) events increases (decreases) when the NAO index is positive. Sproson et al. (2008) suggested that significantly more easterly tip jets occurred in the winter of 1995/1996 when the NAO was in a strongly positive phase. Våge et al. (2009) also found that the

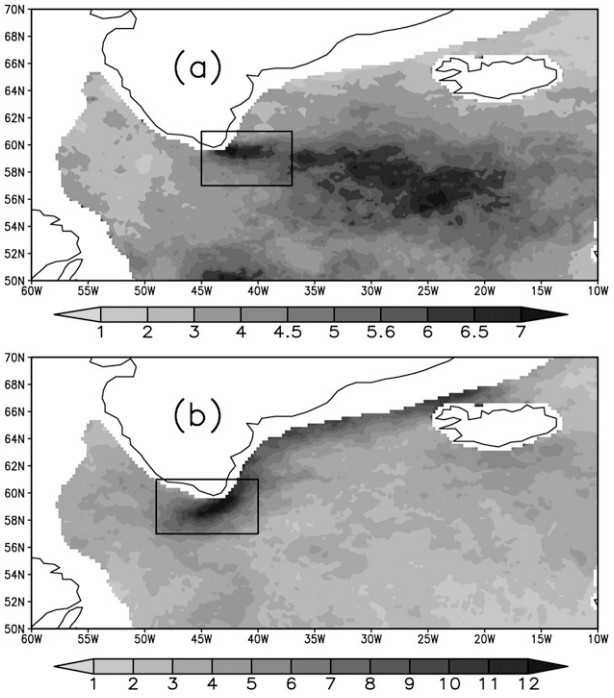

FIG. 10. Interannual standard deviation of winter high-wind frequency (%) associated with (a) westerly wind and (b) easterly wind from QuikSCAT data.

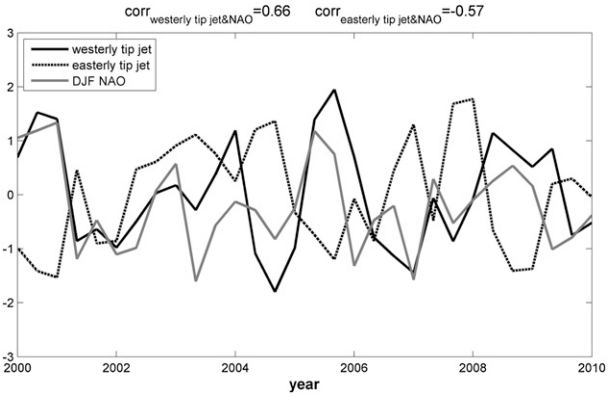

FIG. 11. Time series of westerly high wind frequency (averaged in black rectangle in Fig. 10a), easterly high-wind frequency (averaged in black rectangle in Fig. 10b), and the NAO index. All time series are normalized by their respective standard deviations and have been detrended using linear least squares regression.

number of westerly tip jet events detected from the 40-yr European Centre for Medium-Range Weather Forecasts Re-Analysis (ERA-40) has a significant positive correlation with the NAO. However, few studies have used satellite data to study the interannual variability of HWF in this region.

Figure 10 displays the interannual standard deviation of westerly and easterly HWFs calculated from the same dataset used in Fig. 9. The maximum standard deviation of westerly HWF is found southeast of Cape Farewell and south of Iceland. There is a narrow band of enhanced STD that extends from Cape Farewell toward the east, with a value of about 7% (Fig. 10a). The STD of easterly HWF is even higher with a value of about 12% off Cape Farewell (Fig. 10b). As shown in Fig. 11, westerly HWF variability off Cape Farewell is significantly correlated with the NAO index ($r = 0.66$), while easterly HWF variability is negatively correlated with the NAO index at -0.57 (Fig. 11b). During a positive NAO winter, there are stronger westerly winds in the subpolar North Atlantic Ocean, as well as a more northeasterly storm track and a greater number of synoptic systems passing near Greenland (Rogers 1990; Hurrell et al. 2003), which favors westerly high-wind events off Cape Farewell. When the NAO index is negative, storm tracks are found at lower latitudes with the cyclone centers south of Cape Farewell (Moore 2003; Trigo 2006), in favor of the easterly high wind occurrence off Cape Farewell. The opposite impact of the NAO on westerly and easterly HWF explains the poor correlation between the NAO index and HWF off Cape Farewell derived from SSM/I data. Although the occurrence of westerly and easterly HWF correlates well with the NAO, the correlation is not as high as in the area south of Iceland, which indicates other climate modes may be also important.

5. Summary and discussion

We have studied interannual variability of HWF over the North Atlantic using measurements from SSM/I and QuikSCAT. We show that the SSM/I data capture the major features of HWF fairly well in comparison to the Sampe and Xie (2007) analysis using QuikSCAT. Remarkable seasonal variability of HWF is found over the Atlantic Ocean. High wind occurs most frequently in winter and its frequency exceeds 10% in the vicinity of the Gulf Stream, off Cape Farewell, and in the open ocean south of Iceland. The strong westerly winds, storm-track intensity, SST front in winter, and coastal orography contribute to HWF in these regions. High wind occurs less frequently in spring and autumn since the storm-track intensity and mean westerlies weaken. In summer, the HWF is close to zero over the whole basin.

Interannual variability of HWF is then investigated using 22-yr SSM/I wind speed data. High interannual variability of HWF is found over open sea south of Iceland, off Cape Farewell, and in the vicinity of the Gulf Stream—a distribution similar to the climatology. On interannual scales, HWF south of Iceland displays a remarkable positive correlation with the NAO ($r = 0.71$). When the NAO index is positive, an increase in

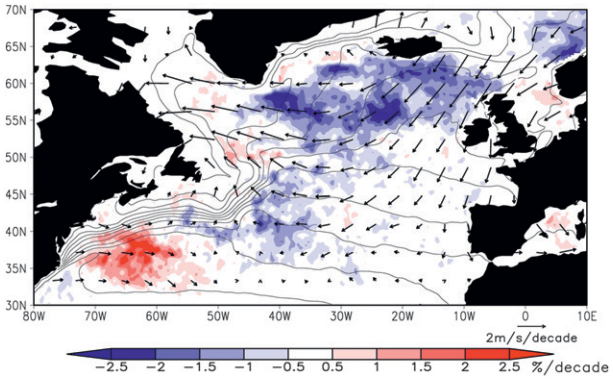

FIG. 12. Local trend of high wind frequency (color) and 10-m wind (vector) over 1988–2009 superimposed on climatological seasonal means of AVHRR SST (black contours, 2°C intervals).

the mean westerlies and storm track intensity contributes to the increase in HWF in this region. Along the Gulf Stream front, HWF has significant correlations with SST − SAT, indicating the importance of atmospheric instability. Cross-frontal wind and an SST gradient are important for the instability of MABL on the warm flank of the SST front (Wallace et al. 1989; Xie 2004). A high correlation coefficient between cross-frontal cold advection ($\mathbf{U} \cdot \nabla T$) and atmospheric instability (SST − SAT) in the vicinity of the SST front indicates that the aforementioned mechanisms are also valid on interannual time scales. The EA mode is found to be the primary driver of the interannual variations of HWF in regions B and C.

The region near Cape Farewell is recognized as the windiest place in the world's oceans (Sampe and Xie 2007; Moore et al. 2008). Westerly and easterly high winds occur alternately in this region. Without distinguishing the HWF induced by two types of high wind, the total HWF off Cape Farewell derived from SSM/I exhibits a poor correlation with the NAO index. Using the QuikSCAT data, we then find westerly HWF off Cape Farewell has a significant positive correlation with NAO ($r = 0.66$), while easterly HWF is negatively correlated with the NAO index ($r = -0.57$). This result is consistent with previous studies of tip jet variability based on NCEP and ERA-40 reanalyses (Moore 2003; Våge et al. 2009).

Previous studies suggest that the NAO index displays substantial decadal trends: positive from the 1960s to early 1990s and negative afterward (Hurrell 1995; Gruber 2009; Lozier et al. 2008). Decadal changes in the atmospheric circulation during winter in the North Atlantic are strongly related to the NAO (Hurrell 1995). In response to the phase change of NAO, surface westerlies over the North Atlantic Ocean have significantly weakened during 1988–2009 except on the warm flank of the Gulf Stream south of 40°N (Fig. 12). These westerly trends are consistent with a tripole pattern of scalar wind trends observed during this weakening period of NAO (Wentz et al. 2007; Tokinaga and Xie 2011). Weaker westerlies can cause less occurrence of high wind, as illustrated by the negative trend in HWF over the northern North Atlantic. The largest negative trend is found south of Iceland (2.5% decade^{-1}). On the warm flank of the Gulf Stream front off the U.S. East Coast, HWF has increased at a rate of about 2.5% decade^{-1} (Fig. 12) because of the strengthened westerlies.

Besides HWF, surface wind convergence, enhanced evaporation/precipitation, and frequent cloud occurrence are also found on the warm flank of SST fronts (O'Neill et al. 2003; Xie 2004; Minobe et al. 2008; Tokinaga et al. 2009; Kuwano-Yoshida et al. 2010). The present work reveals the effect of cross-frontal cold advection on surface high wind occurrence along the Gulf Stream on interannual time scales. Other atmospheric responses to the Gulf Stream on interannual or even longer-time scales are an interesting subject to be investigated.

Acknowledgments. The SSM/I and QuikSCAT data are produced by Remote Sensing Systems (www.remss.com), with support from the NASA Earth Science MEaSUREs DISCOVER Project and the NASA Ocean Vector Winds Science Team. This work is supported by NASA, NOAA, JAMSTEC, the National Basic Research Program of China (2010CB950303, 2010CB950302), the Natural Science Foundation of China (40806004), and the Qianren and Changjiang Scholar Programs. Part of XHC's work is performed at IPRC on a Chinese Academy of Science Overseas Fellowship. Constructive remarks by two anonymous reviewers are greatly appreciated.

REFERENCES

Barnston, A. G., and R. E. Livezey, 1987: Classification, seasonality, and persistence of low-frequency atmospheric circulation patterns. *Mon. Wea. Rev.,* **115,** 1083–1126.

Barthelmie, R. J., and S. C. Pryor, 2003: Can satellite sampling of offshore wind speeds realistically represent wind speed distributions? *J. Appl. Meteor.,* **42,** 83–94.

Booth, J. F., L. A. Thompson, J. Patoux, K. A. Kelly, and S. Dickinson, 2010: The signature of the midlatitude tropospheirc storm tracks in the surface winds. *J. Climate,* **23,** 1160–1174.

Chelton, D. B., and S.-P. Xie, 2010: Coupled ocean–atmosphere interaction at oceanic mesoscales. *Oceanography,* **23,** 52–69.

——, and Coauthors, 2001: Observations of coupling between surface wind stress and sea surface temperature in the eastern tropical Pacific. *J. Climate,* **14,** 1479–1498.

——, M. G. Schlax, M. H. Freilich, and R. F. Milliff, 2004: Satellite measurements reveal persistent small-scale features in ocean winds. *Science,* **303,** 978–983.

Deser, C., and M. L. Blackmon, 1993: Surface climate variations over the North Atlantic Ocean during winter: 1900–89. *J. Climate,* **6,** 1743–1753.

Doyle, J. D., and M. A. Shapiro, 1999: Flow response to large-scale topography: The Greenland tip jet. *Tellus,* **51,** 728–748.

Gruber, N., 2009: Fickle trends in the ocean. *Nature,* **458,** 155–156.

Hashizume, H., S.-P. Xie, W. T. Liu, and K. Takeuchi, 2001: Local and remote atmospheric response to tropical instability waves: A global view from space. *J. Geophys. Res.,* **106,** 10 173–10 185.

Hollinger, J. P., 1989: *DMSP Special Sensor Microwave/Imager Calibration/Validation: Final Report*. Vol. I, Space Sensing Branch, Naval Research Laboratory, 419 pp.

Hoskins, B. J., and K. I. Hodges, 2002: New perspectives on the Northern Hemisphere winter storm tracks. *J. Atmos. Sci.,* **59,** 1041–1061.

Hurrell, J. W., 1995: Decadal trends in the North Atlantic Oscillation: Regional temperatures and precipitation. *Science,* **269,** 676–679.

——, Y. Kushnir, M. Visbeck, and G. Ottersen, 2003: An overview of the North Atlantic Oscillation. *The North Atlantic Oscillation: Climatic Significance and Environmental Impact, Geophys. Monogr.,* Vol. 134, Amer. Geophys. Union, 1–35.

Josey, S. A., and R. Marsh, 2005: Surface freshwater flux variability and recent freshening of the North Atlantic in the eastern subpolar gyre. *J. Geophys. Res.,* **110,** C05008, doi:10.1029/2004JC002521.

Kalnay, E., and Coauthors, 1996: The NCEP/NCAR 40-Year Reanalysis Project. *Bull. Amer. Meteor. Soc.,* **77,** 437–471.

Kuwano-Yoshida, A., S. Minobe, and S.-P. Xie, 2010: Precipitation response to the Gulf Stream in an atmospheric GCM. *J. Climate,* **23,** 3676–3698.

Lin, I., and Coauthors, 2003: New evidence for enhanced ocean primary production triggered by tropical cyclone. *Geophys. Res. Lett.,* **30,** 1718, doi:10.1029/2003GL017141.

Liu, W. T., X. Xie, P. S. Polito, S.-P. Xie, and H. Hashizume, 2000: Atmospheric manifestation of tropical instability wave observed by QuikSCAT and Tropical Rainfall Measuring Mission. *Geophys. Res. Lett.,* **27,** 2545–2548.

Lozier, M. S., S. J. Leadbetter, R. G. Williams, V. Roussenov, M. S. C. Reed, and N. J. Moore, 2008: The spatial pattern and mechanisms of heat content change in the North Atlantic. *Science,* **319,** 800–803.

Minobe, S., A. Kuwano-Yoshida, H. Tokinaga, S.-P. Xie, and R. J. Small, 2008: Influence of the Gulf Stream on the troposphere. *Nature,* **452,** 206–209.

Moore, G. W. K., 2003: Gale force winds over the Irminger Sea to the east of Cape Farewell, Greenland. *Geophys. Res. Lett.,* **30,** 1894, doi:10.1029/2003GL018012.

——, and I. A. Renfrew, 2005: Tip jets and barrier winds: A QuikSCAT climatology of high wind speed events around Greenland. *J. Climate,* **18,** 3713–3725.

——, R. S. Pickart, and I. A. Renfrew, 2008: Buoy observations from the windiest location in the world ocean, Cape Farewell, Greenland. *Geophys. Res. Lett.,* **35,** L18802, doi:10.1029/2008GL034845.

Nonaka, M., and S.-P. Xie, 2003: Covariations of sea surface temperature and wind over the Kuroshio and its extension: Evidence for ocean-to-atmosphere feedback. *J. Climate,* **16,** 1404–1413.

O'Neill, L. W., D. B. Chelton, and S. K. Esbensen, 2003: Observations of SST-induced perturbations of the wind stress field over the Southern Ocean on seasonal timescales. *J. Climate,* **16,** 2340–2354.

Outten, S. D., I. A. Renfrew, and G. N. Petersen, 2009: An easterly tip jet off Cape Farewell, Greenland. II: Simulations and dynamics. *Quart. J. Roy. Meteor. Soc.,* **135,** 1934–1949.

Pezzoli, A., G. Tedeschi, and F. Resch, 2004: Numerical simulation of strong wind situations near the French Mediterranean coast: Comparison with FETCH data. *J. Appl. Meteor.,* **43,** 997–1015.

Pickart, R. S., M. A. Spall, M. H. Ribergaard, G. W. K. Moore, and R. F. Milliff, 2003: Deep convection in the Irminger Sea forced by the Greenland tip jet. *Nature,* **424,** 152–156.

Renfrew, I. A., and Coauthors, 2008: The Greenland flow distortion experiment. *Bull. Amer. Meteor. Soc.,* **89,** 1307–1324.

——, S. D. Outten, and G. W. K. Moore, 2009: An easterly tip jet off Cape Farewell, Greenland. Part I: Aircraft observations. *Quart. J. Roy. Meteor. Soc.,* **135,** 1919–1933.

Reynolds, R. W., N. A. Rayner, T. M. Smith, D. C. Stokes, and W. Wang, 2002: An improved in situ and satellite SST analysis for climate. *J. Climate,* **15,** 1609–1625.

——, T. M. Smith, C. Liu, D. B. Chelton, K. S. Casey, and M. G. Schlax, 2007: Daily high-resolution blended analyses for sea surface temperature. *J. Climate,* **20,** 5473–5496.

Risien, C. M., and D. B. Chelton, 2006: A satellite-derived climatology of global ocean winds. *Remote Sens. Environ.,* **105,** 221–236.

Rogers, D. P., 1989: The marine boundary layer in the vicinity of an ocean front. *J. Atmos. Sci.,* **46,** 2044–2062.

Rogers, J. C., 1990: Patterns of low-frequency monthly sea level pressure variability (1899–1986) and associated wave cyclone frequencies. *J. Climate,* **3,** 1364–1379.

——, 1997: North Atlantic storm track variability and its association to the North Atlantic Oscillation and climate variability of northern Europe. *J. Climate,* **10,** 1635–1645.

Sampe, T., and S.-P. Xie, 2007: Mapping high sea winds from space: A global climatology. *Bull. Amer. Meteor. Soc.,* **88,** 1965–1978.

Small, R. J., S.-P. Xie, and Y. Wang, 2003: Numerical simulation of atmospheric response to Pacific tropical instability waves. *J. Climate,* **16,** 3722–3740.

——, and Coauthors, 2008: Air–sea interaction over ocean fronts and eddies. *Dyn. Atmos. Oceans,* **45,** 274–319.

Soloviev, A., and R. Lukas, 2006: *The Near-Surface Layer of the Ocean: Structure, Dynamics and Applications*. Springer, 572 pp.

Spall, M. A., 2007: Midlatitude wind stress–sea surface temperature coupling in the vicinity of oceanic fronts. *J. Climate,* **20,** 3785–3801.

Sproson, D. A. J., I. A. Renfrew, and K. J. Heywood, 2008: Atmospheric conditions associated with oceanic convection in the southeast Labrador Sea. *Geophys. Res. Lett.,* **35,** L06601, doi:10.1029/2007GL032971.

Tanimoto, Y., and S.-P. Xie, 2002: Inter-hemispheric decadal variations in SST, surface wind, heat flux and cloud cover over the Atlantic Ocean. *J. Meteor. Soc. Japan,* **80,** 1199–1219.

Thum, N., K. E. Steven, D. B. Chelton, and J. M. McPhaden, 2002: Air–sea heat exchange along the northern sea surface temperature front in the eastern tropical Pacific. *J. Climate,* **15,** 3361–3378.

Tokinaga, H., and S.-P. Xie, 2011: Wave- and anemometer-based sea surface wind (WASWind) for climate change analysis. *J. Climate,* **24,** 267–285.

——, Y. Tanimoto, and S.-P. Xie, 2005: SST-induced surface wind variations over the Brazil–Malvinas confluence: Satellite and in situ observations. *J. Climate,* **18,** 3470–3482.

——, ——, ——, T. Sampe, H. Tomita, and H. Ichikawa, 2009: Ocean frontal effects on the vertical development of clouds

over the western North Pacific: In situ and satellite observations. *J. Climate,* **22,** 4241–4260.

Trigo, I. F., 2006: Climatology and interannual variability of storm-tracks in the Euro-Atlantic sector: A comparison between ERA-40 and NCEP/NCAR reanalyses. *Climate Dyn.,* **26,** 127–143.

Våge, K., T. Spengler, H. C. Davies, and R. S. Pickart, 2009: Multi-event analysis of the westerly Greenland tip jet based upon 45 winters in ERA-40. *Quart. J. Roy. Meteor. Soc.,* **135,** 1999–2011.

Visbeck, M., J. W. Hurrell, L. Polvani, and H. M. Cullen, 2001: The North Atlantic Oscillation: Past, present, and future. *Proc. Natl. Acad. Sci. USA,* **98,** 12876–12877.

——, E. P. Chassignet, R. G. Curry, T. L. Delworth, R. R. Dickson, and G. Krahmann, 2003: The ocean's response to North Atlantic Oscillation variability. *The North Atlantic Oscillation, Climatic Significance and Environmental Impact, Geophys. Monogr.,* Vol. 134, Amer. Geophys. Union, 113–146.

Wallace, J. M., T. P. Mitchell, and C. Deser, 1989: The influence of sea surface temperature on surface wind in the eastern equatorial Pacific: Seasonal and interannual variability. *J. Climate,* **2,** 1492–1499.

Warner, T. T., M. N. Lakhtakia, and J. Doyle, 1990: Marine atmospheric boundary layer circulations forced by Gulf Stream sea surface temperature gradients. *Mon. Wea. Rev.,* **118,** 309–323.

Wentz, F. J., 1997: A well-calibrated ocean algorithm for special sensor microwave/imager. *J. Geophys. Res.,* **102,** 8703–8718.

——, D. K. Smith, C. A. Mears, and C. L. Gentemann, 2001: Advanced algorithms for QuikScat and SeaWinds/AMSR. *Proc. Int. Geoscience and Remote Sensing Symp. 2001,* Vol. 3, Sydney, Australia, IEEE, 1079–1081.

——, L. Ricciardulli, K. Hilburn, and C. Mears, 2007: How much more rain will global warming bring? *Science,* **317,** 233–235.

Worley, S. J., S. D. Woodruff, R. W. Reynolds, S. J. Lubker, and N. Lott, 2005: ICOADS release 2.1 data and products. *Int. J. Climatol.,* **25,** 823–842.

Xie, S.-P., 2004: Satellite observations of cool ocean–atmosphere interaction. *Bull. Amer. Meteor. Soc.,* **85,** 195–208.

——, M. Ishiwatari, H. Hashizume, and K. Takeuchi, 1998: Coupled ocean–atmospheric waves on the equatorial front. *Geophys. Res. Lett.,* **25,** 3863–3866.

Yuan, X., 2004: High-wind-speed evaluation in the Southern Ocean. *J. Geophys. Res.,* **109,** D13101, doi:10.1029/2003JD004179.